



**HAL**  
open science

## A novel approach to the study of extensional flow-induced crystallization

Juliana Amirdine, Thouaïba Htira, Nicolas Lefevre, René Fulchiron, Nathalie Mathieu, Matthieu Zinet, Christophe Sinturel, Teodor Burghelea, Nicolas Boyard

► **To cite this version:**

Juliana Amirdine, Thouaïba Htira, Nicolas Lefevre, René Fulchiron, Nathalie Mathieu, et al.. A novel approach to the study of extensional flow-induced crystallization. *Polymer Testing*, 2021, 96, pp.107060. 10.1016/j.polymertesting.2021.107060 . hal-03113971v2

**HAL Id: hal-03113971**

**<https://hal.science/hal-03113971v2>**

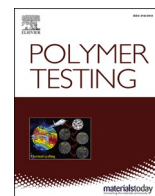
Submitted on 29 Jan 2025

**HAL** is a multi-disciplinary open access archive for the deposit and dissemination of scientific research documents, whether they are published or not. The documents may come from teaching and research institutions in France or abroad, or from public or private research centers.

L'archive ouverte pluridisciplinaire **HAL**, est destinée au dépôt et à la diffusion de documents scientifiques de niveau recherche, publiés ou non, émanant des établissements d'enseignement et de recherche français ou étrangers, des laboratoires publics ou privés.



Distributed under a Creative Commons Attribution - NonCommercial - NoDerivatives 4.0 International License



## A novel approach to the study of extensional flow-induced crystallization

Juliana Amirdine<sup>a</sup>, Thouaïba Htira<sup>b</sup>, Nicolas Lefevre<sup>a</sup>, René Fulchiron<sup>b</sup>, Nathalie Mathieu<sup>c</sup>,  
Matthieu Zinet<sup>b</sup>, Christophe Sinturel<sup>c</sup>, Teodor Burghilea<sup>a</sup>, Nicolas Boyard<sup>a,\*</sup>

<sup>a</sup> Université de Nantes, CNRS, Laboratoire de Thermique et Energie de Nantes, UMR 6607, La Chantrerie, Rue Christian Pauc, F-44000, Nantes, France

<sup>b</sup> Univ Lyon, Université Claude Bernard Lyon 1, CNRS, IMP UMR 5223, F-69622, Villeurbanne, France

<sup>c</sup> Interfaces, Confinement, Matériaux et Nanostructures (ICMN), UMR 7374, CNRS-Université D'Orléans, CS 40059, F-45071, Orléans, France

### ARTICLE INFO

#### Keywords:

Extensional flow

Flow induced crystallization

Modified SER fixture

### ABSTRACT

A systematic experimental investigation of the coupling between the extensional flow and the crystallization of a commercial grade polypropylene is presented. A modified Sentmanat extensional device allows one to generate a uniaxial extensional flow in the absence of gravity sagging and monitoring its effect on the kinetics of crystallization via in-situ visualization of the sample in polarised light. As compared to the shear induced crystallization, a three fold increase of the kinetics of the extension induced crystallization is found. The study is complemented by a post mortem analysis of the crystalline morphology by small angle X ray scattering (SAXS) and wide angle X ray scattering (WAXS).

### 1. Introduction

Polymer forming processes such as injection molding, extrusion or film blowing are widely used in the plastic industry. During the forming process, the plastic undergoes a phase change which takes place under different conditions of pressure, flow and cooling rate. The processing conditions (pressure [1]; cooling rate [2,3] and flow [4,5] impact the crystallization phenomenon in terms of its kinetics and crystalline microstructure. The phenomenon of flow-induced crystallization (FIC) has been widely studied in the literature [6–8]. Beyond a critical shear rate the shear-induced crystallization (SIC) shows an acceleration of the kinetics manifested through an increase in the number of nuclei [4,8,9]. The flow also impacts the microstructure by orienting it along its direction which sometimes leads to the formation of a highly oriented microstructure called shish-kebab [5,10,11].

In the case of polypropylene which is a polymorphic polymer the flow may also lead to the formation of the  $\beta$ -phase in addition to the classical  $\alpha$ -phase, [12]. In addition, some authors show that the processing conditions accelerate the associated crystallization kinetics [13–15]. These kinetics are of primary importance for the process simulation. Thus, appropriate models need to be developed and used in order to describe various processing settings. The modification of the microstructure and the kinetics of crystallization under flow need to be accounted for in order to simulate polymer processing operations. While crystallization in quiescent conditions is easily modelled by the well

known formalism of Avrami [16–18]; the flow induced crystallization remains elusive and new models need to be developed [19]. Suggests taking into account the flow from a differential approach or the work of Peters [11] or that of Haudin-Chenot [20] may explain the presence of different crystalline phases.

The extension is the dominant flow during many polymer processing operations including melt blowing, extrusion and fibre spinning, [21–23]. Unlike shear flows, extensional flows are clearly more complex and their laboratory implementation is rather non trivial. Quite often, one can not generate a purely extensional flow but a mixture of shear and extension. Several devices used to study the response of polymeric materials to extensional flow were then developed: the Rheometrics Melt Rheometer (RME) by Meissner [24]; the Münstedt Tensile Rheometer (MTR) by Münstedt [25]; or the Sentmanat Extensional Rheometer (SER) [22] and the Filament Stretching Rheometer (FISER) [26–28]. Among these devices, only the SER tool is commercially available and can be easily mounted on any rotational rheometer.

As opposed to the case of shear flow, there exist very few studies of the coupling between crystallization and the extensional flow. This might be explained by the fact that in order to study the crystallization a number of modifications of the extensional devices are needed. As an example, Bischoff White and coworkers have studied the extension induced crystallization using a modified FISER device, [15]. They observe an acceleration of kinetics of crystallization for extensional rates exceeding a critical value. Other studies I propose the construction of

\* Corresponding author.

E-mail address: [Nicolas.Boyard@univ-nantes.fr](mailto:Nicolas.Boyard@univ-nantes.fr) (N. Boyard).

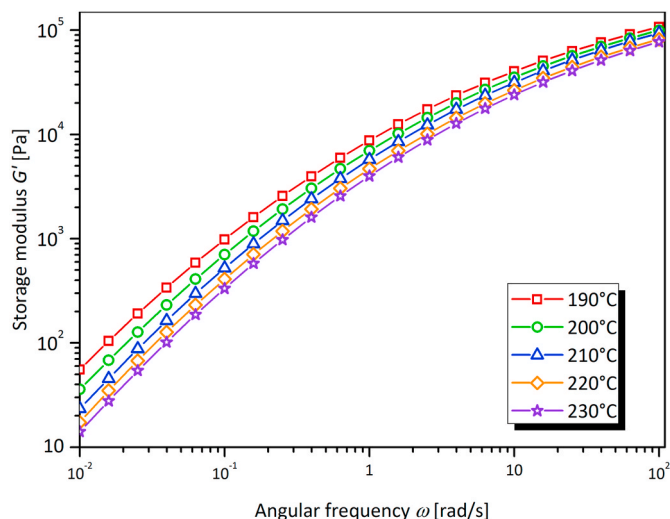


Fig. 1. Dependence of the storage modulus  $G'$  on the oscillation frequency measured for several temperatures  $T$  indicated in the insert.

new extensional setups inspired by the SER, [29–32]. A heating system using ionic liquid combined with optically transparent walls allows an *in-situ* analysis of the crystalline microstructure during extension. However, these studies do not address the coupling before the microstructure and the kinetics of crystallization.

There exist few studies dealing with this coupling [14,15,29–34]. Their studies show a mainly *post-mortem* or *in-situ* characterization of the crystalline microstructure using classical DSC and X-ray scattering techniques (SAXS and WAXS). The extension generates a strong orientation of the crystalline lamellae in the direction of flow and an increase in the number of nuclei. However, a quantitative assessment of the kinetics of crystallization and its relation to the properties of the extensional flow is largely absent in the literature. Such an assessment is of paramount importance for developing a theoretical framework for the EIC and its further numerical implementation. The present study proposes a systematic experimental characterization of the crystallization induced by extensional flow in both an *in-situ* and *post-mortem* fashion. The use of polarized light *in-situ* characterization tool allows one to assess the characteristic time scales associated to the crystallization and to compare them with the times of semi-crystallization obtained in either quiescent conditions or during a shear flow. The characterization of the microstructure and of the induced crystal phases is also performed.

The paper is organised as follows. The choice of the working polymeric material and the description of the experimental methods are detailed in Sec. 2. The experimental results are presented in Sec. 3. The crystallization in quiescent conditions is discussed in Sec. 3.1. The shear induced crystallization is investigated in Sec. 3.2. The extension induced crystallization is studied in Sec. 3.3. The assessment of the extension induced crystallization via classical measurements of the transient elongational viscosity is presented in Sec. 3.3.1. An *in-situ* characterisation of the crystallization process by means of polarised light imaging of the sample undergoing an extensional deformation is presented in Sec. 3.3.2. A systematic investigation of the impact of the extensional conditions on the crystalline micro-structure by means of wide angle X-ray scattering (WAXS) and small angle X-ray scattering performed post mortem is presented in Sec. 3.3.3. The paper closes with a summary of the main findings and of the central conclusions of the study, Sec. 4.

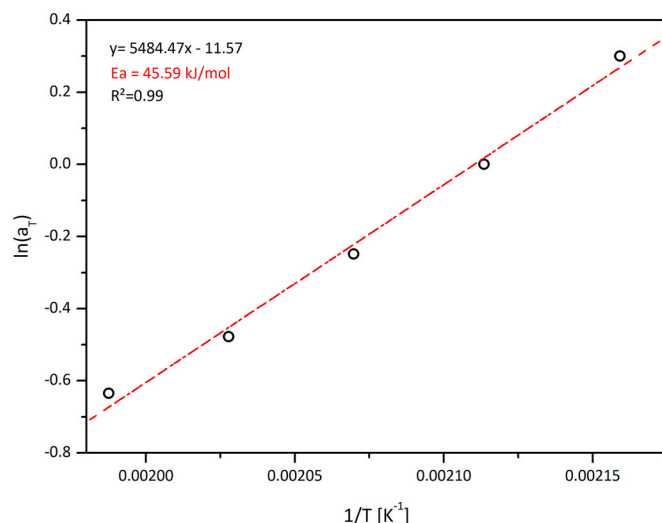


Fig. 2. Dependence of the shift factor on temperature. The full line is a linear fit function  $\ln(a_T) = a(\pm\delta a)\frac{1}{T} + b(\pm\delta b)$ .

## 2. Experimental methods

### 2.1. Choice of the polymeric material

The study of the extension induced crystallization was performed using a commercial grade isotactic polypropylene (iPP) from Lyondell-Basell (MOPLENHP556E). The choice of this linear iPP was mainly motivated by its high molecular weight of  $M_w = 527\text{kg/mol}$  which translates into a good sensitivity to extensional flow. In addition to this, this material is known to exhibit a relatively modest strain hardening behaviour under extensional flow which allows one to relate an apparent increase of the transient extensional viscosity to the flow induced crystallization. The polydispersity index is 5.3 [35] and the quiescent melting temperature is  $T_m = 164^\circ\text{C}$ .

### 2.2. Rheological characterisation in shear

The linear viscoelastic (LVE) properties of the iPP were determined using a strain-controlled rheometer Ares G2 (TA Instruments) equipped with a 25mm parallel plate geometry. Dynamic frequency sweeps were performed (100 to 0.01rad/s,  $\gamma = 5\%$ ) under nitrogen atmosphere at several temperatures ranging from 190°C to 230°C. Measurements of the storage modulus performed various temperatures are illustrated in Fig. 1.

The master curve was determined at 200°C from an Arrhenius plot of the vertical shift factor  $a_T$  versus the inverse temperature  $1/T$ . In order to extract the activation energy from these measurements, a reference temperature  $T = 200^\circ\text{C}$  has been chosen and the vertical shift factors  $a_T$  required to overlap the rest of the data sets onto the reference one have been obtained. The temperature dependence of the shift factors is illustrated in Fig. 2. The activation energy was found by fitting the dependence of the vertical shift factors on temperature by an Arrhenius law (the full line in Fig. 2)  $E_a = 45.59\text{kJ/mol}$  (Fig. 2) which is in a fair agreement with results previously reported in the literature [8].

Last, the master curve was fitted by a  $N$ -mode ( $N = 5$ ) Maxwell model (Eq. (2)).

$$G'(\omega) = \sum_{i=1}^N G_i \frac{(\omega\lambda_i)^2}{1 + (\omega\lambda_i)^2} \quad (1)$$

$$G''(\omega) = \sum_{i=1}^N G_i \frac{\omega\lambda_i}{1 + (\omega\lambda_i)^2} \quad (2)$$

**Table 1**  
Relaxation spectrum for *iPP* at 200°C.

$\lambda_i$ [s]	$G_i$ [Pa]
$(2.8 \pm 2) \cdot 10^{-2}$	$(7.1 \pm 0.45) \cdot 10^4 Pa$
$(2.5 \pm 5) \cdot 10^{-2}$	$(2.7 \pm 0.33) \cdot 10^4 Pa$
$(1.9 \pm 0.24)$	$(5.9 \pm 0.4) \cdot 10^3 Pa$
$(1.4 \pm 0.2) \cdot 10^1$	$(6.9 \pm 1.2) \cdot 10^2 Pa$
$(1.1 \pm 0.5) \cdot 10^2$	$(3.8 \pm 0.8) \cdot 10^1 Pa$

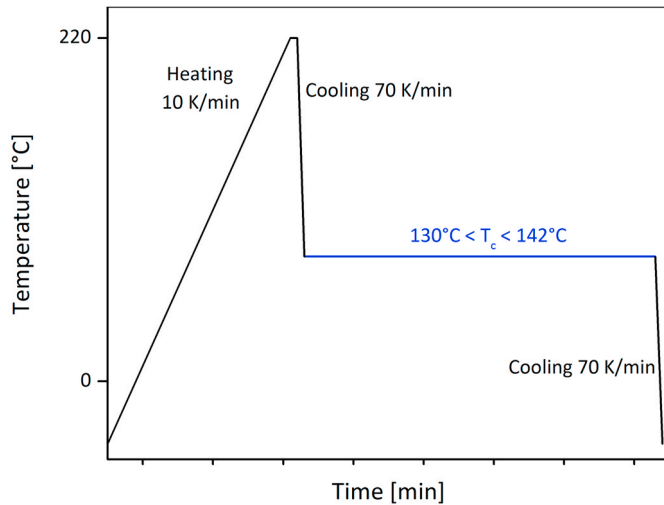


Fig. 3. Diagram of the temperature cycle for DSC apparatus.

The parameters relaxation moduli  $G_i$  and the relaxation times  $\lambda_i$  are listed in Table 1. The average relaxation time given by  $\lambda_w = \frac{\sum G_i \lambda_i^2}{\sum G_i \lambda_i}$  was  $\lambda_w = 19.3s$  at 200°C.

### 2.3. Quiescent crystallization (QC)

The kinetics of crystallization in quiescent conditions were investigated on a sample of approximately 7.5mg using Differential Scanning Calorimetry (DSC) (model Q200 from TA Instruments). The experimental protocol is presented Fig. 3. On this device, the achievable cooling speed is approximately 70K/min. Thus, thanks to DSC, the crystallization kinetics of PP can be obtained in a range of temperatures between 130 and 142°C because crystallization should not appear during cooling.

The relative crystallinity is determined by integrating the heat flux according to Eq. (3) where  $\phi$  is the heat flux released at a given time and  $\Delta H_{tot}$  the totale enthalpy of crystallization. The half-crystallization time  $t_{1/2}$  was obtained for a relative crystallinity  $\alpha = 0.5$ . The initial time  $t = 0$  was defined as the moment where the isothermal condition was reached.

$$\alpha(t) = \frac{\int_0^t \phi(\tau) d\tau}{\Delta H_{tot}} \quad (3)$$

To assess the kinetics of crystallization at lower temperatures, Fast Scanning Calorimetry (FSC) [36–38] is performed in a nitrogen gas atmosphere using a Flash DSC1 from Mettler Toledo. The mass of the sample is roughly 1μg. FSC achieves much faster cooling rates than DSC and enables to impose a PP quenching rate (cooling) of 2000K/s. Thus, the kinetics of crystallization of PP can be obtained according to the same protocol as in DSC but ranging from 5 and 110°C. When the heat

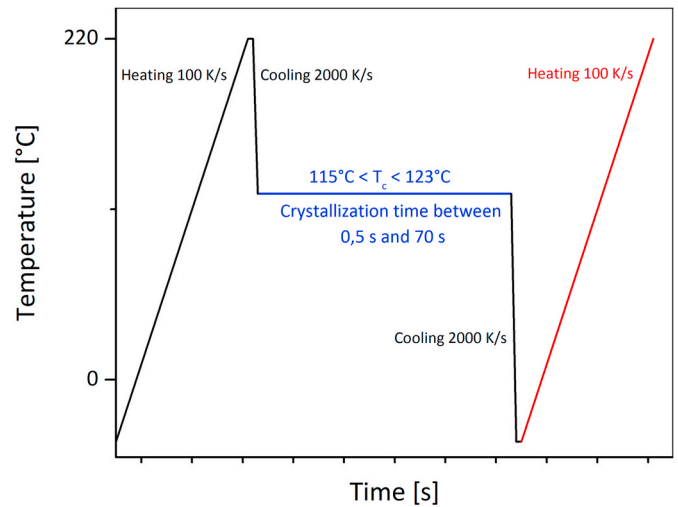


Fig. 4. Experimental protocol for the discrete method in FSC.

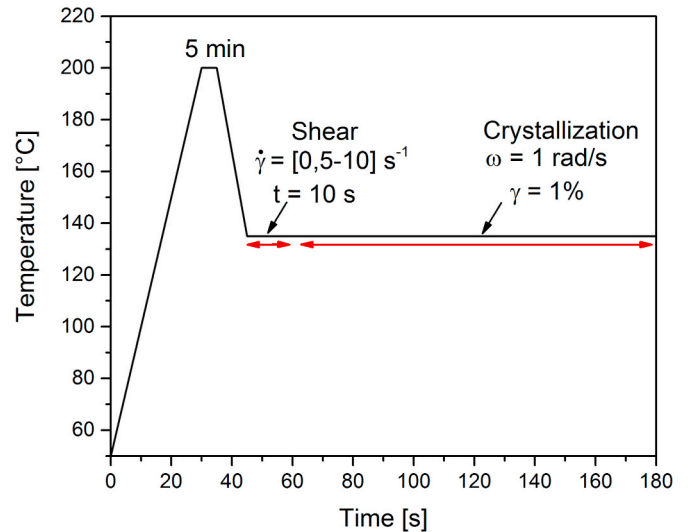


Fig. 5. Diagram of the temperature cycle.

flux is too low, the discrete method described by Ref. [39] is used. It consists on repeating the isothermal crystallization while changing crystallization time. The melting enthalpy determined during the heating step is equivalent to the measure of the crystallization enthalpy during the previous isothermal step (Fig. 4).

Thanks to the DSC and FSC measurements, the kinetics of crystallization of PP can be studied by determining the half-crystallization time over a large temperature range.

### 2.4. Shear induced crystallization (SIC)

To study shear flow, the classical Janeschitz-Kriegl thermal protocol was used (Fig. 5).

The shear induced crystallization (SIC) was studied using the same rheometer used for the rheological characterisation in shear. The polymer pellets were first maintained at 220°C for 5min in a 8mm diameter cone-plate 0.1rad geometry with a gap equal to 0.051mm. Then the sample was cooled down as fast as possible to the expected temperature (isothermal condition). For each temperature, a shear rate between 0.5s<sup>-1</sup> to 10s<sup>-1</sup> was applied for  $t_s = 10s$ , a time which is high enough to have a significant effect on the orientation of the macromolecular chains [12,40]. The crystallization was tracked through the response of the

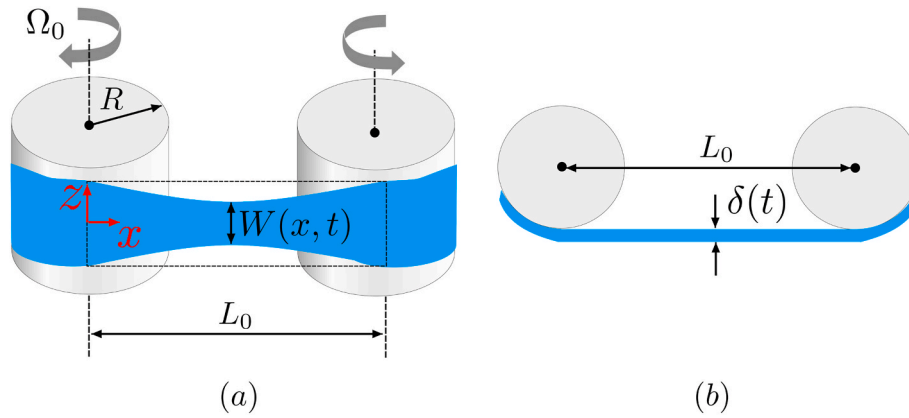


Fig. 6. Schematic view of the Sentmanat extensional rheometer (SER) during operation.

sample to an oscillatory strain with a frequency  $\omega = 1\text{rad/s}$  ( $\gamma = 1\%$ ). The experiments were carried on under nitrogen gas to avoid thermal oxydation of the iPP. The half-crystallization time was estimated according to the semi-empirical rule proposed by Ref. [12] to:

$$\log G'_{t_{1/2}} = \frac{\log(G'_{max}) + \log(G'_{min})}{2} \quad (4)$$

The gap is adjusted in real time to avoid the experimental artefacts induced by the shrinkage of the sample during the crystallization process. The onset time of crystallization  $t_{onset}$  was defined by the time corresponding to an increase of the storage modulus.

### 2.5. Extensional-flow induced crystallization (EIC)

A Sentmanat Extensional Rheometer (SER) [22] device was installed on a Haake Mars III rheometer (from ThermoFischer Scientific) to study the extensional-flow Induced crystallization (EIC). It consists on two rotating cylindrical drums of radius  $R$  separated by a distance  $L_0$ . They were inter-coupled by a system of gears such as the rotation of the cylinder connected to the shaft triggers the rotation of the second cylinder at a same angular speed but in an opposite direction (Fig. 6). For all the experiments reported herein a rectangular sample with dimensions  $18\text{mm} \times 10\text{mm} \times 0.50\text{mm}$  was used. The iPP sample was moulded by compression at  $200^\circ\text{C}$  for 5 min to erase the thermal history and then cooled down at  $140^\circ\text{C}$ . The sample was then fixed on the outer surface of the rotating cylinders with two thin stainless steel clamps. For a constant angular speed of the shaft of the rotational rheometer,  $\Omega$ , the Hencky strain rate experienced by the sample is expressed according to Eq. (5):

$$\dot{\epsilon}_H = \frac{2\Omega R}{L_0} \quad (5)$$

The transient uniaxial extensional viscosity is defined as  $\eta_e^+ = \frac{\sigma_e^+(t)}{\dot{\epsilon}_H}$  where the transient extensional stress  $\sigma_e^+$  is defined as:

$$\sigma_e^+(t) = \frac{M}{2RA(t)\exp(-\dot{\epsilon}_H t)} \quad (6)$$

In the equation above  $M$  is the torque measured by the rotational rheometer,  $A(t)$  is the cross-sectional area of the sample as a function of temperature:

$$A(t) = A_0 \exp\left(\frac{\rho_s}{\rho_m(T)}\right)^{2/3} \quad (7)$$

where  $\rho_s$  is the sample density at solid state ( $845\text{kg/m}^3$  at  $20^\circ\text{C}$ ),  $\rho_m(T)$  is the melt density at temperature  $T$  (determined from PvT diagram; as an example, at  $200^\circ\text{C}$   $\rho_m(T)$  is equal to  $748\text{kg/m}^3$ ), and  $A_0$  is the initial cross-sectional area of the sample. The total deformation of the sample is limited to a maximum Hencky strain of  $\dot{\epsilon}_H^{max} = 4$  because the fixing clamps come into contact after three-quarter turn. The measurements were carried out at Hencky strain rates from  $0.05\text{s}^{-1}$  to  $10\text{s}^{-1}$ .

The Sentmanat device was initially designed for the characterisation of elastomers rather than of polymer melts [22]. When used with molten polymeric samples there are two important drawbacks to be aware of. First, the samples are heated using a convection oven mounted on the rotational rheometer. Thus, the homogeneity of the temperature distribution of the sample may be problematic and, for the commercially available ovens, practically impossible to assess quantitatively. Second, as the sample is held in air, gravity sagging effects bias the extensional tests particularly in a range of low rates of extension [22,29]. As the walls of the oven are not optically transparent, the geometric homogeneity of the sample can not be visually assessed.

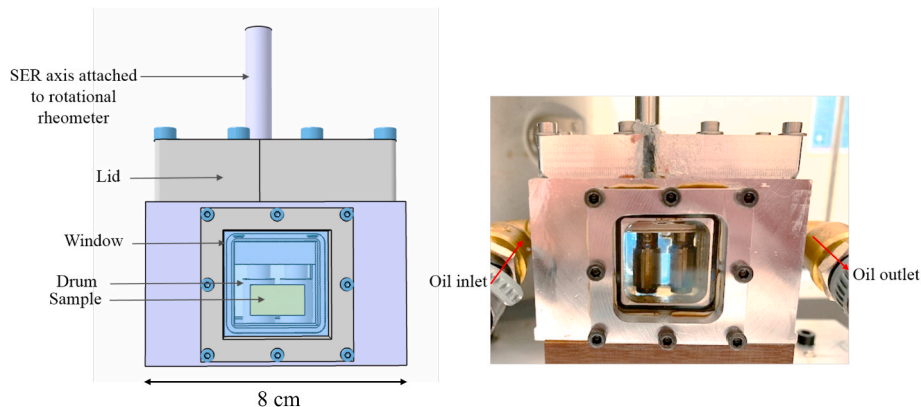


Fig. 7. Schematic and real view of the Sentmanat extensional rheometer (SER) during operation.

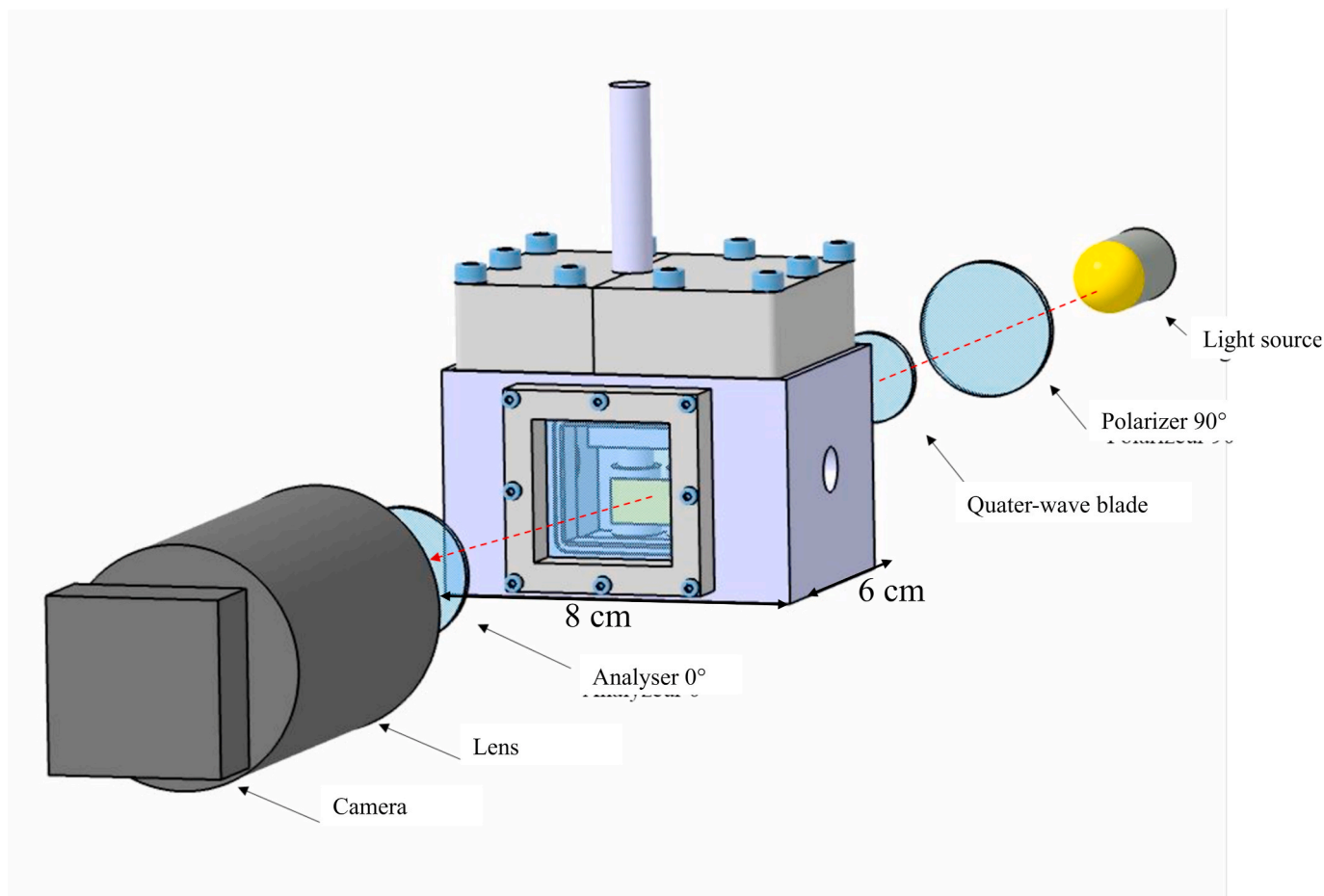


Fig. 8. Schematic representation of the polarised light imaging system.

To circumvent these practical limitations, a custom-made oil bath to submerge the Sentmanat device was fitted to the rotational rheometer (Fig. 7). Through the bath with a volume 65mL thermally stabilised, silicon oil is continuously circulated which plays three important roles. First, this addition allows one to ensure a homogeneous distribution of temperature within the sample. Second, as the density of the silicon oil is close to that of the molten polymeric sample, the gravity sagging effects are practically eliminated. This experimental trick was already used by other authors [25,29] and the question of possible interaction between the liquid and the specimen was never addressed. The use of the liquid with a density similar to the sample one is the only way to avoid the gravity sagging effect.

Third and foremost, the front/back glass windows of the oil bath allow an *in-situ* analysis of the extension induced crystallization by means of polarised light imaging of the sample during extension. The temperature cycle performed in SIC is retained (Fig. 5), however the cooling rate remains slower (10K/min) in the case of EIC measurements due to the thermoregulation capability of the oil bath.

## 2.6. *In-situ and post-mortem quantitative assessment of the extension induced crystallization*

### 2.6.1. *In-situ visualization with polarised light*

An *in-situ* quantitative assessment of the extension induced crystallization is made by direct imaging of the sample in polarised light during the extensional process. The optical arrangement is inspired by Refs. [41,42] and is schematically illustrated in Fig. 8 and may be described as follows. The sample is illuminated from behind through the back glass window of the oil bath by a white light source. Prior to traversing the

sample, the white light is passed through a polarizer (90°, 400 – 700nm) and a quarter-wave plate. The light is collected through the front glass window of the oil bath by an analyzer (0°, 400 – 700nm) oriented at  $\pi/2$  with respect to the polarisation axis of the polarizer and projected onto the sensor of a digital charged coupled device equipped with an appropriate focusing lens.

The kinetics of crystallization is quantitatively assessed by monitoring the intensity of the light received by the video camera (Chameleon, Flir) during the extensional flow experiment. The image acquisition process is synchronised with the data acquisition one performed by the rotational rheometer. The recording continues after the extensional flow. The light intensity is determined by a home-made matlab code (image processing toolbox) allowing the average of the gray levels determined in a fixed area of the image between the cylinders of the SER.

### 2.6.2. *X-ray measurements*

SAXS experiments were performed on a high resolution X-ray spectrometer Xeuss 2.0 from Xenocs company equipped with a 30W micro-focus sealed tube (Cu target ( $\lambda = 1.5418\text{\AA}$ )). The X-ray spot size on sample is about 1 mm and the incident flux of  $6 \cdot 10^6$  photons per second. The SAXS patterns were recorded with a 2D high intensity low noise detector (Pilatus 300K hybrid pixel) placed at a distance of 2373mm from the sample, perpendicular to the X-ray beam (pixel size =  $172\mu\text{m}$ ). The size of X-ray beam on sample is about 1mm. The 2DSAXS patterns were recorded post-mortem after removing the extended sample from the SER device in a solid state. 1DSAXS profiles were extracted using FIT2D software within a q-range  $0.08 - 1.7\text{nm}^{-1}$ . and 1D profiles were corrected from background, incident flux, sample thickness (0.3mm),

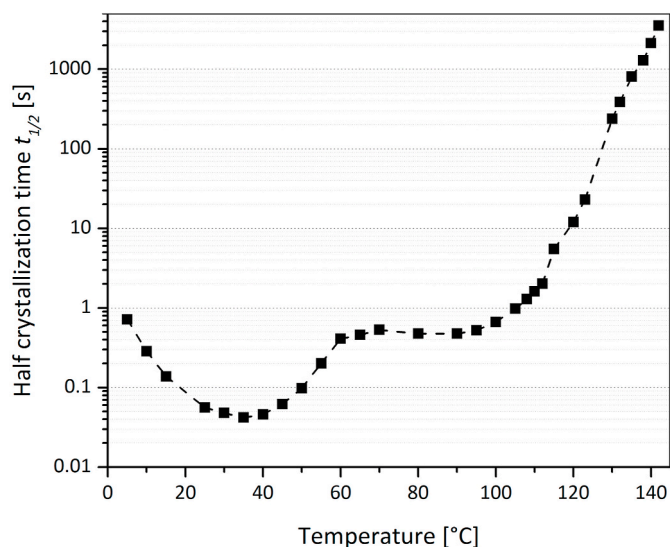


Fig. 9. Half-crystallization time in quiescent condition obtain by DSC and Flash DSC.

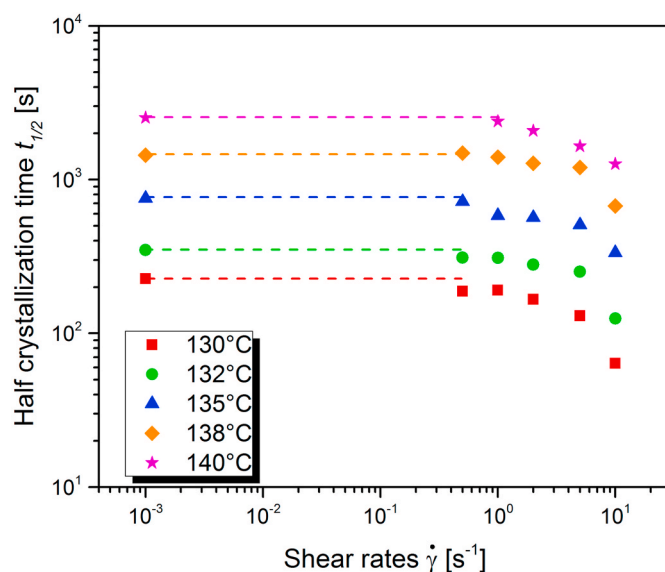


Fig. 11. Half time crystallization for different pre-shear rates ( $t_s = 10s$ ) and temperatures. The dotted lines illustrate a plateau over which, the crystallization is not affected by the pre-shear rate.

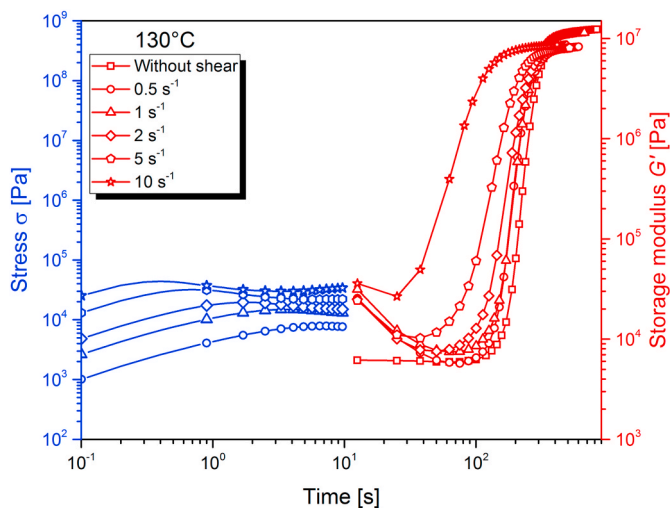


Fig. 10. Isothermal crystallization monitored by the evolution of the elastic modulus after a pre-shearing step of 10s performed for several imposed rates of shear and at  $T_c = 130^\circ C$ .

acquisition time (5 h) and solid angle of detection  $\Omega$ . The long period of the crystalline lamellae is called  $L_p$  and was estimated by  $L_p = \frac{2\pi}{q_{max}}$  [1].

Wide Angle-X-ray diffraction (WAXS) was performed at center of Diffractométrie Henri Longchambon (UCBL, Université Lyon 1) using a Oxford system with a copper source (wavelength of 1.54 Å). In order to determine the crystalline orientation, measurements were performed in transmission. The tube supplies 40eV and 30mA. The exposure time was 390s. The data were analyzed using the software Datasqueeze (1D integration and plots as a function of azimuthal angle).

### 3. Experimental results, discussion

#### 3.1. Crystallization in quiescent conditions

The crystallization of the PP has been widely studied in quiescent conditions [8,43–46] using DSC and FSC. We describe in the following similar measurements performed with PP samples crystallised in quiescent conditions. Following the protocols detailed in the previous section, the half-crystallization time versus temperature is plotted in

Fig. 9.

According to Refs. [45,46]; *iPP* exhibits a bimodal kinetics with a phase transition at  $65^\circ C$ . The  $\alpha$ -phase, the most stable phase, is formed for low or medium supercooling at a crystallization temperature higher than  $70^\circ C$  and for which the kinetics becomes faster. Below this limit, a mesophase is formed from a homogeneous nucleation mechanism and the half-crystallization time is increasing due to a low chain mobility. Unlike the  $\alpha$ -phase, the mesophase is much less ordered or is considered even disordered by same authors [45].

#### 3.2. Shear-induced crystallization

The experimental results of the study of shear-induced crystallization are summarised in Fig. 10. The horizontal axis is divided in two distinct parts. The first one corresponds to an imposed shear for 10s. The stress level (blue curves) increases with the shear rates. During the second stage of the tests after 10s (red curves), apart from the curve labelled as *emph* "without shear", one observes first a drop in the storage modulus. This can be explained in terms of a relaxation of the polymer chains. Then, the curve of the storage modulus exhibits a shape which is qualitatively similar to the curve describing the evolution of the relative crystallinity, since it follows a sigmoidal evolution. The onset time of crystallization and the half-crystallization time can be determined from this part of the curve. Non-shear experiment was performed showing a good agreement with the half-crystallization times obtained in DSC in quiescent condition.

The dependence of the half-crystallization time on the rate of shear plotted in Fig. 11 exhibits a plateau region for the quiescent half-crystallization time (positioned at  $\dot{\gamma} = 10^{-3}s^{-1}$ ) up to about  $1s^{-1}$  followed by a decrease of the half-crystallization time independently on the temperature. One notes that a critical shear rate exists beyond which the kinetics of cristallization is accelerated,  $\dot{\gamma}_c \approx 4s^{-1}$ . This behaviour is well known in the literature basing on the onset time of the storage modulus increase for a polyethylene by Ref. [4] or a poly-1-butene by Ref. [9]. [8, 47] made the same observation for the half-crystallization time for a PP and a polyamide respectively.

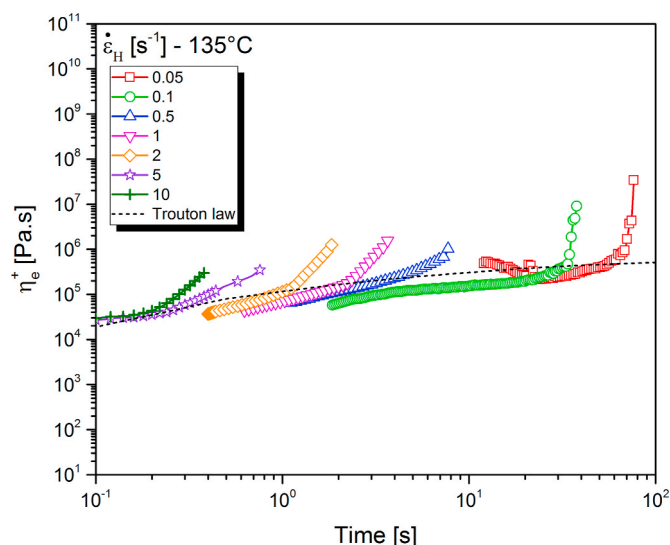


Fig. 12. Extensional viscosity at 135°C for different Hencky strain rates, the black dashed line represents the linear viscoelastic response obtained by Trouton's law.

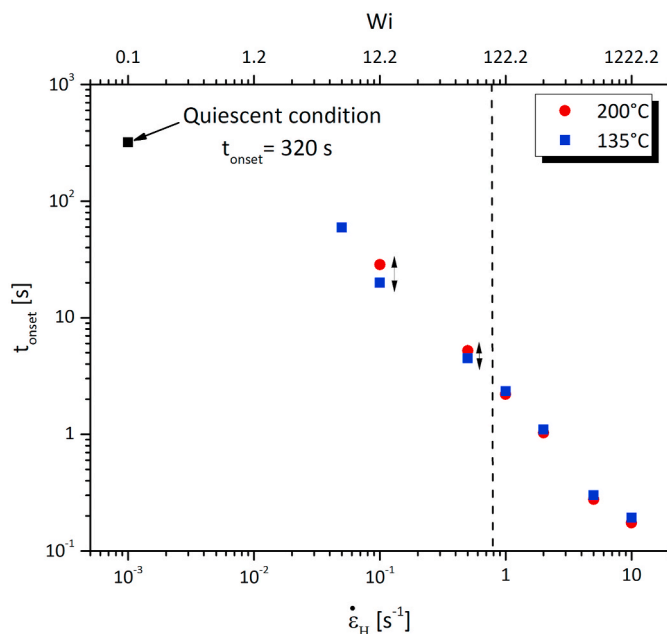


Fig. 13. Onset time measured at 200°C (circles) and 135°C (squares) for different Hencky strains. The corresponding Weissenberg numbers are displayed on the top axis.

### 3.3. Crystallization under extensional flow

#### 3.3.1. Measurements of the transient extensional viscosity

Fig. 12 presents the extensional viscosity at 135°C for different Hencky strain rates and a Hencky strain of  $\epsilon_H = 4$ . For each rate of extension, the extensional viscosity changes in a similar way, until a sudden increase in the extensional viscosity called strain-hardening. The Trouton's law represents the linear viscoelastic response for uniaxial extension and is given by  $\eta_e^+ = 3\eta_0$  where  $\eta_0$  is the viscosity obtained from rotational rheometry in the newtonian domain. For temperatures below the melting temperature, it is not possible to carry out a frequency sweep over long times because crystallization would appear. Therefore, the Trouton's law is calculated according to the Maxwell model ( $n_i =$

$G_i\lambda_i$ ), whose parameters are given in Table 1:

$$\eta_e^+ = 3 \sum_{i=1}^N n_i \left[ 1 - \exp\left(-\frac{\dot{\epsilon}_H}{n_i}\right) \right] \quad (8)$$

A strain-hardening behaviour is observed for all the rates of extension  $\dot{\epsilon}_H$  investigated. The intensity of strain-hardening increases when the rates of extension decrease. This behaviour depends on the molar mass of the molten, polymer as highlighted by Ref. [48].

[33] suggests to plot the onset times of strain-hardening increase as a function of the extension rate to quantify the presence of crystallization. The onset of strain-hardening (or crystallization) is determined when the extensional viscosity deviates from the Trouton's law. Fig. 13 compares the onset time at 200°C and 135°C versus the Hencky strain rates and the Weissenberg number ( $Wi = \dot{\epsilon}_H \times \lambda_w$ ). The onset time  $t_{onset}$  in quiescent conditions indicated in the figure is the time of the beginning of crystallization obtained by DSC during an isothermal step at 135°C. At 200°C, *iPP* is completely molten while at 135°C crystallization may occur.  $t_{onset}$  decreases linearly with the increase of the extension rate. A slight effect of the temperature on the onset times may be observed only for the smallest Hencky strain rates (lower than  $1s^{-1}$ ) we have explored which correspond to the longest experimental time. Based on this macroscopic observation, one could assume that crystallization occurs for numbers  $Wi$  smaller than 122 at 135°C. For low Hencky strain rates, the macromolecular chains are stretched longer and remain longer in the oil bath, inducing a possible effect of crystallization on the extensional viscosity for these extension rates in addition to the strain-hardening. However, this analysis can be discussed because crystallization could also start well before the apparition of strain-hardening. On the contrary, for higher rates of extension, the measurement time is decreasing, so it is possible that it is not long enough to recover an effect of the crystallization on the extensional viscosity. With the SER tool the tensile force can only be recorded during the flow, not after.

Finally, it is clear that it is not possible to conclude definitely about crystallization, based on the extensional viscosity curves only. At this point, we believe that the crystallization occurs after the elongation.

#### 3.3.2. In situ characterization by using polarized light

The oil bath and the polarised light imaging system allow one to follow the crystallization *in-situ* by monitoring the intensity of the flow induced birefringence *FIB*. The measurements are carried out at 133°C up to a final Hencky strain of 2.5 so as not to obstruct the optical path between the cylindrical drums. The maximal rate of extension achievable with our rheometer is  $\dot{\epsilon}_H^{max} = 2s^{-1}$ . The measured light intensity  $I$  of each subsequent image is measured in a fix rectangle (red dotted lines in Fig. 14) and normalised by the light intensity  $I_0$  measured without the sample. Images of the sample acquired during and after extension and the light intensity are illustrated in Figs. 14 and 15, respectively.

First, an increase of the light intensity is observed during the application of the extensional flow. This can be explained first by the decrease of the thickness of the sample (0.51mm to 0.30 mm) during the test. However, this behaviour was also observed during the SIC experiments. The extensional flow aligns the polymer chains, thus creating an optically anisotropic behaviour named flow induced birefringence (*FIB*). Moreover, the light intensity increases more and more with the Hencky strain rate. Indeed, the extension mechanism is exponential in time unlike shear. The extensional flow therefore aligns the chains more, which promotes nucleation, or even strongly oriented microstructures.

At the end of the extensional process, the light intensity decreases due to the relaxation of the macromolecular chains. At this point, it is interesting to correlate this result with the extensional viscosity behaviour; if the crystallization started during extension (or close to the end of extension), the light intensity would continue to increase when stopping the elongational flow, but not decrease. Therefore, the difference of onset times previously mentioned is not related to the crystallization phenomenon. Note that the intensity does not come back to the



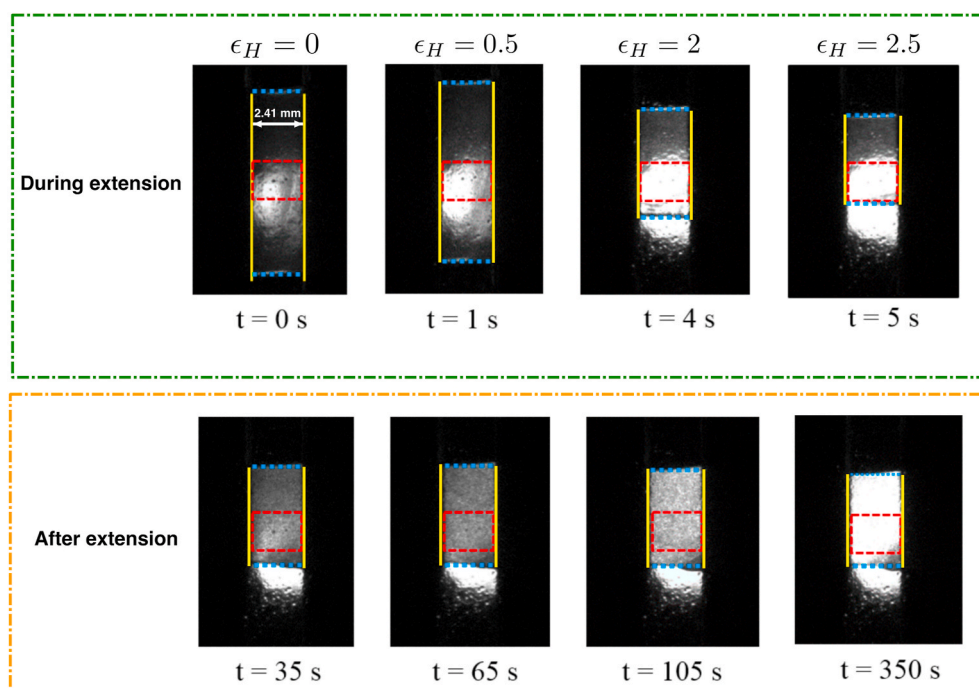


Fig. 14. Light intensity during and after the extensional flow at 133°C,  $\dot{\epsilon}_H = 0.5s^{-1}$ ,  $\epsilon_H = 2.5$ . The vertical yellow lines mark the positions of the rotating drums and the blue horizontal dashed lines mark the top/bottom edges of the sample. (For interpretation of the references to colour in this figure legend, the reader is referred to the Web version of this article.)

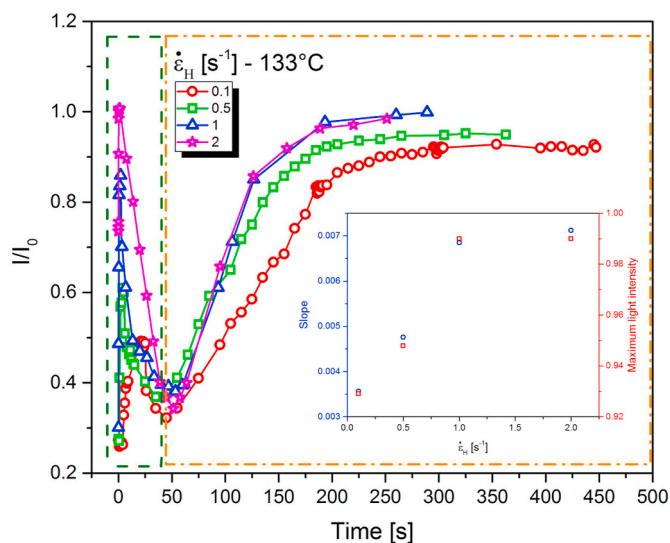


Fig. 15. Light intensity evolution 133°C,  $\dot{\epsilon}_H = 0.5s^{-1}$ ,  $\epsilon_H = 2.5$

initial value, suggesting that all PP macromolecules do not relax (which is confirmed by the mean relaxation time at 133°C,  $\lambda_w = 130.6s$ ) Then, the crystallization is observed through the increase of the light intensity (birefringence induced by the semi-crystalline microstructure) strongly up to a plateau. The value of the plateau depends on the Hencky strain rate: the higher the Hencky strain rate is higher the plateau value is. This may be attributed to a larger orientation of the microstructure and an increase of crystalline fraction. The slope of the light intensity increases with the Hencky strain rate, which suggests a faster kinetics of crystallization. However, the onset time seems to be not affected. The next question relates to understanding how to quantitatively assess the kinetics of crystallization using such measurements and compare the results to those obtained for the case of a shear flow. To do so, we use the

Table 2

Half crystallization times in quiescent condition, after pre-shear and after extension.

T(°C)	$\dot{\gamma}$ or $\dot{\epsilon}_H$ (s <sup>-1</sup> )	Quiescent condition	Shear	SER
		$t_{1/2}(s)$	G (Pa) $t_{1/2}(s)$	I/I <sub>0</sub> $t_{1/2}(s)$
132/133	0.1	388	X	125
	0.5		311	105
	1		310	100
	2		280	100

assumption that  $I/I_0$  is proportional to the relative crystallinity. We mention at this point that we have performed no calibration measurements with a single layer of spherulites (in our case, a thickness of the sample equal to 0.3mm certainly accommodates several such layers). Yet, Koscher and Fulchiron have demonstrated that while monitoring the isothermal crystallization using different methods (DSC, rheometry, polarized light imaging) a good agreement on the values of the half crystallization time  $t_{1/2}$  is obtained, [8]. Based on these considerations we chose to associate the half crystallization time to the time instant when the light intensity augments by 50%. For example, in the case of the experiment performed at an extensional rate of  $0.1s^{-1}$ , the relative light intensity when the crystallization starts is 0.31 whereas its value when full crystallization is achieved is 0.9 which, according to our method, prompts us to chose as a half crystallization time the time instant when the relative intensity is  $I/I_0 = 0.605$ . Nonetheless, the half-crystallization time decreases with  $\dot{\epsilon}_H$  which means that the kinetics of crystallization is faster. The half time of crystallization is estimated around 100s which is significantly lower compared to the value obtained from SIC(300s) and QC measurements (460s) for the same rates ( $0.5s^{-1}$ ) and temperature (133°C).

From all these experiments made under different flow and temperature conditions, we are able to quantify their effect on the crystallization kinetics by comparing the crystallization half-times, as depicted in

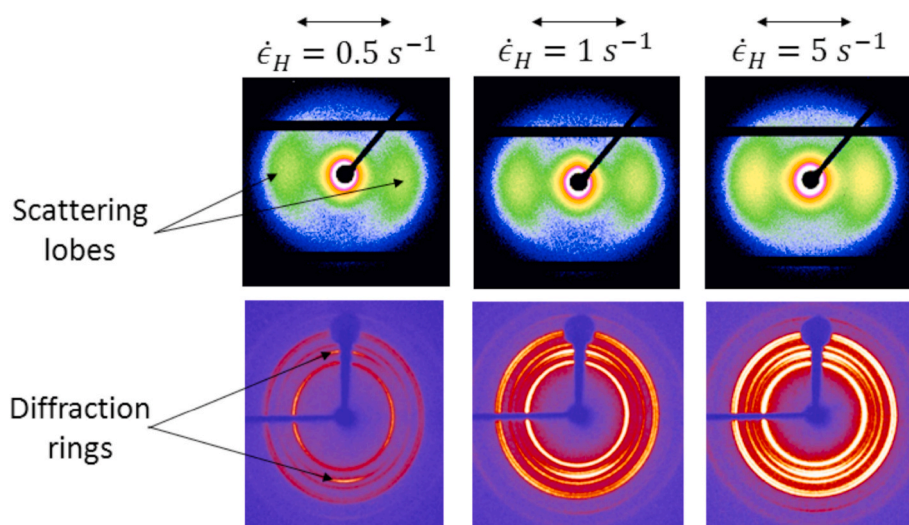


Fig. 16. and 2DWAXS patterns of samples that undergone an extensional flow at  $T = 133^\circ\text{C}$  and several rates of deformation: a)  $\dot{\epsilon}_H = 0.5\text{ s}^{-1}$ , b)  $\dot{\epsilon}_H = 1\text{ s}^{-1}$ , c)  $\dot{\epsilon}_H = 5\text{ s}^{-1}$ . In each panel the arrow indicates the flow direction.

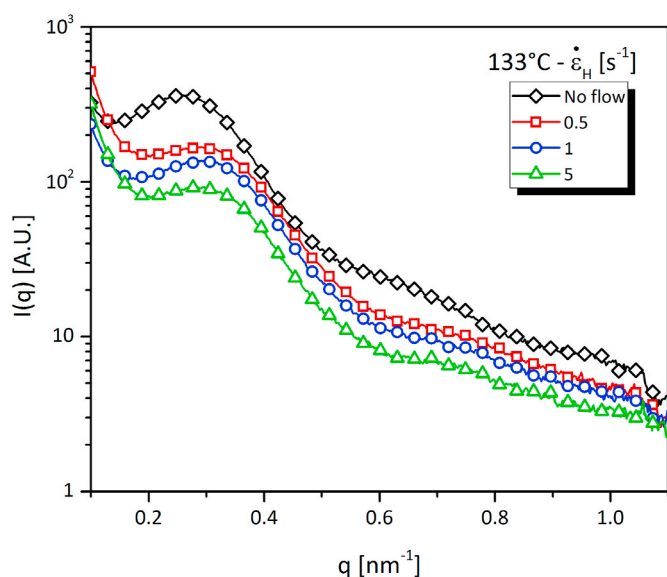


Fig. 17. 1D SAXS data after azimuthal averaging of scattering lobes observed in Fig. 16. The terminal Hencky strain was  $\epsilon_H = 4$ .

Table 2 the comparison of the half-crystallization times shows that the kinetics of crystallization under extensional deformation is divided by a factor 3 compared to the quiescent condition and after a pre-shearing, bringing a quantification of the crystallization induced by extension in an *in-situ* manner.

### 3.3.3. SAXS and WAXS post-mortem measurements

To gain further insights into the role of extension on the crystallization process at microscopic scales, SAXS and WAXS measurements were performed on the polymeric samples after crystallization during extensional flow for a Hencky strain  $\epsilon_H = 4$ . Fig. 16 illustrates SAXS and WAXS measurements performed on PP samples after extension at different  $\dot{\epsilon}_H$  in the middle of the sample, between the two rolls of the SER device. The extension direction is horizontal (equatorial direction) and the X-ray beam intercepted the sample between the two rolls of the SER device where the shrinkage of the cross-section is maximal ( $L_0/2$ ). For all strain rate, SAXS patterns exhibit scattering lobes around the equatorial direction in favour of an orientation of the crystalline lamellae

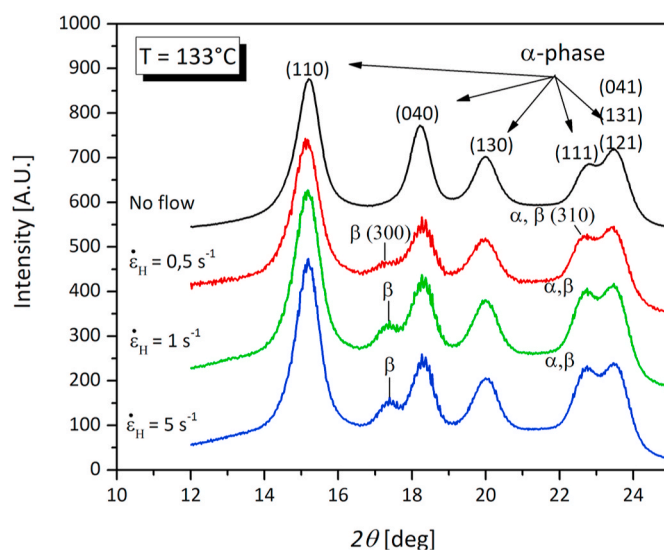


Fig. 18. WAXS patterns measured for different Hencky extension rates at  $133^\circ\text{C}$

perpendicular to the direction of flow. In addition, WAXS indicates the orientation of a crystal plane with the flow by increasing the light intensity of the diffraction rings.

The study of the orientation of each crystalline phase also shows that larger the rate of extension is stronger the orientation is. By comparing the minima and the maxima of the intensity of the scattering peaks versus the azimuthal angle, we observe that the plane (040) of the alpha phase is more oriented than the planes (110) and (300) - see Figs. 22 and 23 in Sec. 6. The stronger orientation of the plane (040) may be explained by the assumption of populations of mother crystalline lamellae and daughter ones which is typically observed with *iPP*. The planes (040) of mother and daughter lamellae are oriented in the same direction whereas the planes (110) of both kinds of lamellae have a double orientation. The WAXS measurements were performed along a single direction of the sample and do not provide information on the orientation of the planes (110) et (300). Thus, to quantify the orientation of the other crystalline planes one needs to perform scattering experiments along several other directions of the sample.

From SAXS patterns, the characteristic size of the lamellar structure

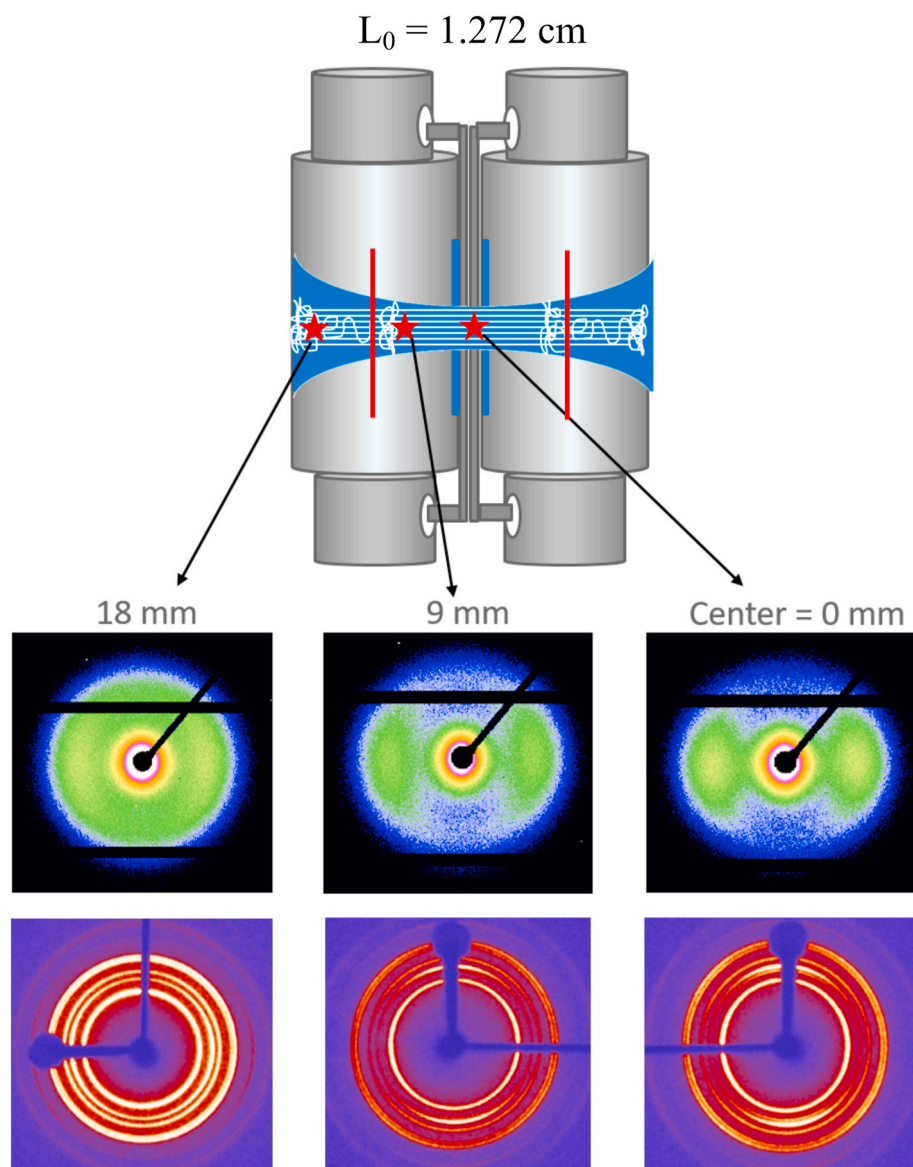


Fig. 19. 2DSAXS and 2DWAXS patterns measured at  $133^{\circ}\text{C}$ ,  $\dot{\epsilon}_H = 1\text{ s}^{-1}$ ,  $\epsilon_H = 4$  and several positions from the centres marked by the stars in the top panel and indicated in the inserts of the lower panels.

is given by the long period  $L_p$  and is defined as  $L_p = \frac{2\pi}{q_{\max}}$ , where  $q_{\max}$  is the value of the wave vector for the scattering peak (see Fig. 17). This value is accurately determined by plotting  $q^2 \times I(q)$  vs.  $q$ . The long period of the un-stretched sample is approximately  $21\text{ nm}$ . In the case of a stretched sample, with increasing extension rates from  $0.5$  to  $5\text{ s}^{-1}$ ,  $L_p$  was found to decrease from  $18.3\text{ nm}$  to  $18.00\text{ nm}$ , which is not significant. Note that for all samples the thermal history remains the strictly the same. Quite obviously,  $L_p$  is not sensitive to the rate of extension but mostly to the presence or absence of flow. The thickness of lamellae is therefore controlled by the temperature.

The WAXS analysis also shows the formation of the  $\beta$ -phase (in addition of the  $\alpha$ -phase) with a higher content when the rate of extension increases as shown in Fig. 18.

A next interesting issue to be addressed is how the microstructure and lamellar orientation revealed by the SAXS and WAXS measurements relates to the horizontal position along the sample. During an experiment, all the polymer flows at the imposed strain rate but the elongational deformation is stopped when it starts to be in contact with the drum. So, after the experiment, the Hencky strain will be maximum ( $\epsilon_H = 4$ ) at the center of the extended sample, whereas it will be smaller

when we move away from this position. At large Hencky strains the sample is slightly narrower close to the centre than close to the edges which implies that the rate of deformation is higher close to the centre and smaller close to the edges as shown in Ref. [49]. To address this question, *post-mortem* SAXS and WAXS measurements were carried out at different positions along the sample as schematically illustrated in the top panel of Fig. 19.

Indeed, the SAXS patterns presented in Fig. 19 clearly indicate that close to the centre of the sample, where the local rate of extension and the Hencky strain are the largest, the orientation is the strongest. This analysis then shows that the deformation is geometrically homogeneous and maximum at this position. Indeed, when approaching the fastening clips, the sample undergoes both shear and extension whereas in the centre of the sample, the sample undergoes pure uniaxial extensional deformation. According to the WAXS measurements, the beta phase appears beyond a critical Hencky strain rate and where the elongation is maximum (at the centre of the sample).

#### 3.3.4. Post mortem DSC measurements

Fig. 20 shows DSC measurements performed on the samples for a

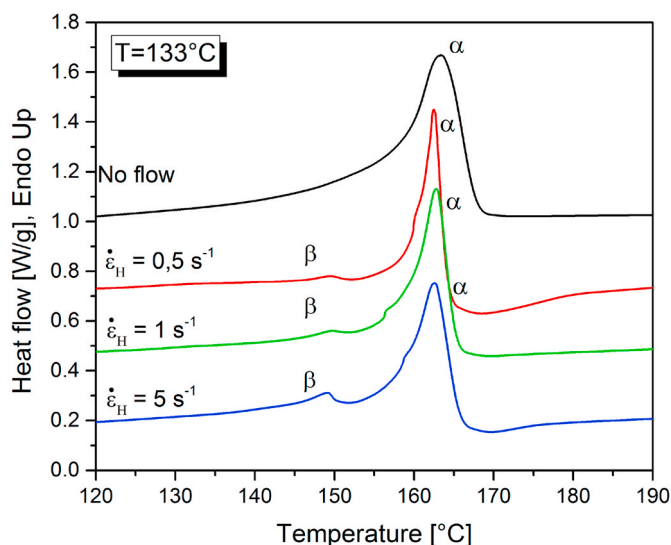


Fig. 20. DSC measurements performed with a sample extended up to Hencky strain  $\varepsilon_H = 4$  at  $9\text{ mm}$  from its centre.

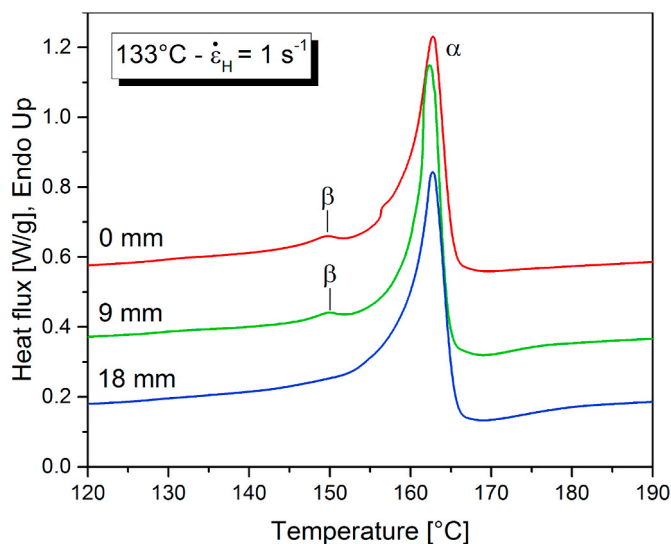


Fig. 21. DSC measurements,  $\varepsilon_H = 4$ ,  $\dot{\varepsilon}_H = 1\text{ s}^{-1}$  for different positions.

deformation of 4 at  $133^\circ\text{C}$ . The black line represents a sample before the extensional flow. Besides, DSC curves present clearly first a main melting peak and also a second one whose intensity increases with the rate. The major melting peak is around a temperature of  $162^\circ\text{C}$  and the minor is around  $148^\circ\text{C}$ . *iPP* is a polymorphic polymer and flow can influence the crystal structure. In quiescent condition, only  $\alpha$ -phase can be observed and for high cooling rates mesophase can also be obtained by FSC [46]. However, under shear flow or extensional flow,  $\beta$ -phase can appear as explained by Ref. [50]. So the major peak is attributed to the  $\alpha$ -phase and the minor to the  $\beta$ -phase according to Ref. [12]; which is also coherent with WAXS data.

As previously shown with SAXS and WAXS measurements, the microstructure and orientation depend on the horizontal position along the sample. Close to the centre (i.e. between the two rolls of SER

apparatus), the orientation is larger since the Hencky strain is larger at this position compared to the other ones, with a homogeneous elongational flow. DSC results (Fig. 21) confirm that the  $\beta$ -phase is more present close to the middle, where extensional deformation is larger and more pure (i.e. no shear is superposed).

#### 4. Conclusions, outlook

A characterization of the crystallization induced by extensional flow is presented. The crystallization of *PP* under quiescent condition and after pre-shear are first presented. This experimental characterization allows one to obtain the half-crystallization times and relate them to the deformation conditions. To study the crystallization induced by extension, a modified SER apparatus is used. The modification consists in equipping the device with an oil bath with transparent walls. This modification allows the *in-situ* visualization of the sample and limits the gravity sagging and ensures a better homogeneity of the temperature distribution within the sample. The kinetics of crystallization was monitored *in-situ* via polarized light imaging of the sample. The estimation of a half-crystallization time indicates an acceleration of the kinetics of crystallization by a factor of 3 as compared to the crystallization under shear. Post-mortem characterization of the samples is performed by both X-ray scattering and DSC measurements. An agreement with previously published results is found. The microstructure is oriented in the direction of flow and the crystalline lamellae are oriented perpendicular to the direction of flow. However, the SAXS measurements indicate no evidence of shish-kebab microstructures. The *post-mortem* analysis also reveals the formation of the  $\beta$  crystalline phase in addition to the majority  $\alpha$  phase. The analysis of the *post-mortem* sample at different axial positions reveals a spatial gradient of the microstructure which is consistent with a gradient of Hencky strain (since the elongation is stopped when the sample is in contact with a roll of the SER apparatus) and an extensional process, which can be slightly kinematically non-uniform.

#### Author contribution

Julana Amirdine: Investigation, Validation, Formal analysis, Writing – original draft, Thouaïba Htira: Investigation, Nicolas Lefevre: Methodology, René Fulchiron: Resources, Writing – review & editing, Nathalie Mathieu: Investigation, Writing – review & editing, Matthieu Zinet: Resources, Christophe Sinturel: Investigation, Teodor Burghelea: Conceptualization, Formal analysis, Writing – original draft, Writing – review & editing, Nicolas Boyard: Conceptualization, Writing – original draft, Writing – review & editing, Supervision, Project administration, Funding acquisition

#### Declaration of competing interest

The authors declare that they have no known competing financial interests or personal relationships that could have appeared to influence the work reported in this paper.

#### Acknowledgements

We gratefully acknowledge the Agence Nationale de la Recherche (ANR) for the financial support via project KinHeTeX (ANR-16-CE08-0022-01). We thank M. Ruben Vera (Centre de Diffractométrie Henri Longchambon, Université Claude Bernard Lyon 1) for WAXS Analyses.

#### Annex

Figs. 22 and 23 show the WAXS intensity as a function of the azimuthal angle for both non-stretched and stretched at  $5\text{ s}^{-1}$  samples, respectively.

Again, the lamellae orientation is revealed by these intensity variations. However, the variation for the 040 peak is much more important than this of the 100 peak. This is generally the case for i-PP when mother-daughter lamellae are present, as shown by Fiorentino and coworkers, [51].

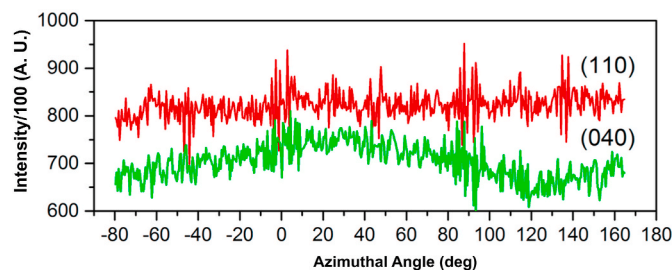


Fig. 22. Dependence of the WAXS intensity on azimuthal angle for the planes (110), (040) (alpha phase) measured after crystallization at 133°C without elongation.

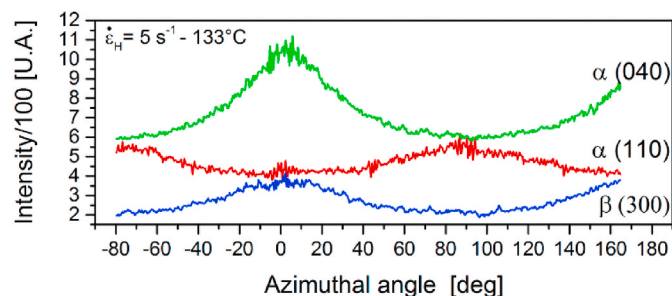


Fig. 23. WAXS intensity versus azimuthal angle for (110), (040) (alpha phase) and (300) (beta phase) planes after crystallization at 133°C for an Hencky strain rate at  $5\text{ s}^{-1}$ . The curves are shifted for better clarity.

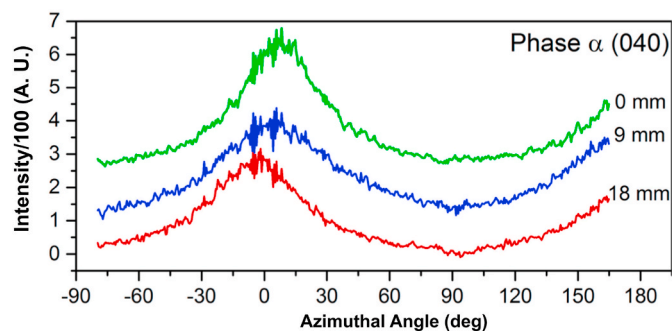


Fig. 24. WAXS intensity versus azimuthal angle for (110), (040) (alpha phase) after crystallization at 133°C for an Hencky strain rate at  $5\text{ s}^{-1}$  for 3 different positions along the specimen: 0mm(center), 9mm and 18mm. The curves are shifted for better clarity.

Fig. 24 shows the WAXS intensity of the 040 peak as a function of the azimuthal angle for the 3 different positions corresponding to different total strains. It appears from the variation amplitudes between  $0^\circ$  and  $90^\circ$  azimuthal angles that the orientation is higher for the position "0" which corresponds to the maximum deformation ( $\epsilon_H = 4$ ).

## References

- [1] C. Angeloz, R. Fulchiron, A. Douillard, B. Chabert, R. Fillit, A. Vautrin, L. David, Crystallization of isotactic polypropylene under high pressure (Gamma phase), *Macromolecules* 33 (2000) 4138–4145, <https://doi.org/10.1021/ma991813e>.
- [2] S.A.E. Boyer, J.M. Haudin, Crystallization of polymers at constant and high cooling rates: a new hot-stage microscopy set-up, *Polym. Test.* 29 (2010) 445–452, <https://doi.org/10.1016/j.polymertesting.2010.02.003>, 10.1016/j.polymertesting.2010.02.003.
- [3] S.A.E. Boyer, P. Robinson, P. Ganet, J.P. Melis, J.M. Haudin, Crystallization of polypropylene at high cooling rates: microscopic and calorimetric studies, *Polym. Polym. Compos.* 125 (2012) 4219–4232, <https://doi.org/10.1002/app>, arXiv: 1206.4529.
- [4] R.R. Lagasse, B. Maxwell, An experimental study of the kinetics of polymer crystallization during shear flow, *Polym. Eng. Sci.* 16 (1976) 189–199, <https://doi.org/10.1002/pen.760160312>, <https://onlinelibrary.wiley.com/doi/abs/10.1002/pen.760160312>, <https://onlinelibrary.wiley.com/doi/pdf/10.1002/pen.760160312>.
- [5] Z. Wang, Z. Ma, L. Li, Flow-induced crystallization of polymers: molecular and thermodynamic considerations, *Macromolecules* 49 (2016) 1505–1517, <https://doi.org/10.1021/acs.macromol.5b02688>.
- [6] G. Eder, H. Janeschitz-Kriegl, S. Liedauer, Crystallization processes in quiescent and moving polymer melts under heat transfer conditions, *Prog. Polym. Sci.* 15 (1990) 629–714, [https://doi.org/10.1016/0079-6700\(90\)90008-0](https://doi.org/10.1016/0079-6700(90)90008-0), <http://www.sciencedirect.com/science/article/pii/0079670090900080>.
- [7] A.J. McHugh, *Flow Induced Crystallization in Polymers in Rheo-Physics of Multiphase Polymeric Systems*, Lancaster ed., Technomic Publishing Co, 1995.
- [8] E. Koscher, R. Fulchiron, Influence of shear on polypropylene crystallization: morphology development and kinetics, *Polymer* 43 (2002) 6931–6942, <https://doi.org/10.1140/epje/12004-10046-8>.
- [9] C. Hadinata, C. Gabriel, M. Ruellman, H.M. Laun, Comparison of shear-induced crystallization behavior of PB-1 samples with different molecular weight distribution, *J. Rheol.* 49 (2005) 327–349, <https://doi.org/10.1122/1.1835342>.
- [10] H. Janeschitz-Kriegl, E. Ratajski, Kinetics of polymer crystallization under processing conditions: transformation of dormant nuclei by the action of flow, *Polymer* 46 (2005) 3856–3870, <https://doi.org/10.1016/j.polymer.2005.02.096>.
- [11] P.C. Roozmond, T.B. Van Erp, G.W. Peters, Flow-induced crystallization of isotactic polypropylene: modeling formation of multiple crystal phases and morphologies, *Polymer* 89 (2016) 69–80, <https://doi.org/10.1016/j.polymer.2016.01.032>, 10.1016/j.polymer.2016.01.032.
- [12] E. Koscher, *Effets du cisaillement sur la cristallisation du polypropylène : aspects cinétiques et morphologiques*, Ph.D. thesis, Université Claude Bernard, Lyon 1, 2002.
- [13] M. Sentmanat, O. Delgadillo-Velázquez, S.G. Hatzikiriakos, Crystallization of an ethylene-based butene plastomer: the effect of uniaxial extension, *Rheol. Acta* 49 (2010) 931–939, <https://doi.org/10.1007/s00397-010-0461-x>.

- [14] M. Derakhshandeh, S.G. Hatzikiriakos, Flow-induced crystallization of high-density polyethylene: the effects of shear and uniaxial extension, *Rheol. Acta* 51 (2012) 315–327, <https://doi.org/10.1007/s00397-011-0605-7>.
- [15] E.E.B. White, H. Winter, J.P. Rothstein, Extensional-flow-induced crystallization of isotactic polypropylene, *Rheol. Acta* 51 (2012) 303–314, <https://doi.org/10.1007/s00397-011-0595-5>.
- [16] M. Avrami, Kinetics of phase change. I - general theory, *J. Chem. Phys.* 7 (1939) 1103–1112.
- [17] M. Avrami, Kinetic of phase change II - transformation-time relations for random distribution of nuclei, *J. Chem. Phys.* 8 (1940) 212–224.
- [18] M. Avrami, Granulation, phase change, and microstructure - kinetics of phase change III, *J. Chem. Phys.* 9 (1941) 177–184.
- [19] W. Schneider, A. Köppl, J. Berger, *Non-Isothermal Crystallization – Crystallization of Polymers – System of Rate Equations*, 1988.
- [20] S.A.E. Boyer, J.P.E. Grolier, H. Yoshida, J.M. Haudin, J.L. Chenot, Thermodynamics and thermokinetics to model phase transitions of polymers over extended temperature and pressure ranges under various hydrostatic fluids, in: J. C. Moreno-Pirajan (Ed.), *Thermodyn. Stud. Gases*, 2011, <https://doi.org/10.5772/823>, <https://www.intechopen.com/books/thermodynamics-interaction-studies-solids-liquids-and-gases/thermodynamics-and-thermokinetics-to-model-phase-transitions-of-polymers-over-extended-temperature-a>.
- [21] S. Muke, I. Ivanov, N. Kao, S.N. Bhattacharya, Extensional rheology of polypropylene melts from the Rheotens test, *J. Nonnewton. Fluid Mech.* 101 (2001) 77–93, [https://doi.org/10.1016/S0377-0257\(01\)00142-2](https://doi.org/10.1016/S0377-0257(01)00142-2).
- [22] M.L. Sentmanat, Miniature universal testing platform: from extensional melt rheology to solid-state deformation behavior, *Rheol. Acta* 43 (2004) 657–669, <https://doi.org/10.1007/s00397-004-0405-4>.
- [23] Z. Stary, M. Papp, T. Burghelca, Deformation regimes, failure and rupture of a low density polyethylene (LDPE) melt undergoing uniaxial extension, *J. Nonnewton. Fluid Mech.* 219 (2015) 35–49, <https://doi.org/10.1016/j.jnnfm.2015.02.007>.
- [24] J. Meissner, J. Hostettler, A new elongational rheometer for polymer melts and other highly viscoelastic liquids, *Rheol. Acta* 33 (1994) 1–21, <https://doi.org/10.1007/BF00453459>.
- [25] H. Münstedt, H.M. Laun, Elongational behaviour of a low density polyethylene melt - II. Transient behaviour in constant stretching rate and tensile creep experiments. Comparison with shear data. Temperature dependence of the elongational properties, *Rheol. Acta* 18 (1979) 492–504, <https://doi.org/10.1007/BF01736955>.
- [26] A. Bach, H.K. Rasmussen, P.Y. Longin, O. Hassager, Growth of non - axisymmetric disturbances of the free surface in the filament stretching rheometer: experiments and simulation, *J. Nonnewton. Fluid Mech.* 108 (2002) 163–186, [https://doi.org/10.1016/S0377-0257\(02\)00129-5](https://doi.org/10.1016/S0377-0257(02)00129-5).
- [27] P. Szabo, G. McKinley, Filament stretching rheometer: inertia compensation revisited, *Rheol. Acta* 42 (2003) 269–272, <https://doi.org/10.1007/s00397-002-0277-4>.
- [28] G. Ianniruberto, G. Marrucci, Y. Masubuchi, Melts of linear polymers in fast flows, *Macromolecules* 53 (2020) 5023–5033, <https://doi.org/10.1021/acs.macromol.0c00693>.
- [29] Y. Liu, W. Zhou, K. Cui, N. Tian, X. Wang, L. Liu, L. Li, Y. Zhou, Extensional rheometer for in situ x-ray scattering study on flow-induced crystallization of polymer, *Rev. Sci. Instrum.* 82 (2011), <https://doi.org/10.1063/1.3574219>, 045104.
- [30] D. Liu, N. Tian, N. Huang, K. Cui, Z. Wang, T. Hu, H. Yang, X. Li, L. Li, Extension-induced nucleation under near-equilibrium conditions: the mechanism on the transition from point nucleus to shish, *Macromolecules* 47 (2014) 6813–6823, <https://doi.org/10.1021/ma501482w>.
- [31] N. Tian, W. Zhou, K. Cui, Y. Liu, Y. Fang, X. Wang, L. Liu, L. Li, Extension flow induced crystallization of poly(ethylene oxide), *Macromolecules* 44 (2011) 7704–7712, <https://doi.org/10.1021/ma201263z>.
- [32] N. Tian, B. Zhao, X. Li, Y. Liu, W. Zhou, K. Cui, D. Liu, L. Li, Confined crystallization in end-linked PEO network under uniaxial extension, *Polymer* 54 (2013) 7088–7093, <https://doi.org/10.1016/j.polymer.2013.10.055>, 10.1016/j.polymer.2013.10.055.
- [33] C. Hadinata, D. Boos, C. Gabriel, E. Wassner, M. Rullmann, N. Kao, M. Laun, Elongation-induced crystallization of a high molecular weight isotactic polybutene-1 melt compared to shear-induced crystallization, *J. Rheol.* 51 (2007) 195, <https://doi.org/10.1122/1.2426977>.
- [34] M. Chellamuthu, D. Arora, H.H. Winter, J.P. Rothstein, Extensional flow-induced crystallization of isotactic poly-1-butene using a filament stretching rheometer, *J. Rheol.* 55 (2011) 901–920, <https://doi.org/10.1122/1.3593471>, <http://sor.scitation.org/doi/10.1122/1.3593471>.
- [35] T.I. Burghelca, H.J. Grieb, H. Münstedt, An in situ investigation of the draw resonance phenomenon in film casting of a polypropylene melt, *J. Nonnewton. Fluid Mech.* 173–174 (2012) 87–96, <https://doi.org/10.1016/j.jnnfm.2012.02.006>, 10.1016/j.jnnfm.2012.02.006.
- [36] S.A. Adamovsky, A.A. Minakov, C. Schick, Scanning microcalorimetry at high cooling rate, *Thermochim. Acta* 403 (2003) 55–63, [https://doi.org/10.1016/S0040-6031\(03\)00182-5](https://doi.org/10.1016/S0040-6031(03)00182-5).
- [37] E. Zhuravlev, C. Schick, Fast scanning power compensated differential scanning nano-calorimeter: 1. The device, *Thermochim. Acta* 505 (2010) 1–13, <https://doi.org/10.1016/j.tca.2010.03.019>, 10.1016/j.tca.2010.03.019.
- [38] E. Zhuravlev, C. Schick, Fast scanning power compensated differential scanning nano-calorimeter: 2. Heat capacity analysis, *Thermochim. Acta* 505 (2010) 1–13, <https://doi.org/10.1016/j.tca.2010.03.020>, 10.1016/j.tca.2010.03.019.
- [39] X. Tardif, B. Pignon, N. Boyard, J.W.P. Schmelzer, V. Sobotka, D. Delaunay, C. Schick, Experimental study of crystallization of PolyEtherEtherKetone (PEEK) over a large temperature range using a nano-calorimeter, *Polym. Test.* 36 (2014) 10–19, <https://doi.org/10.1016/j.polymertesting.2014.03.013>, 10.1016/j.polymertesting.2014.03.013.
- [40] S. Karpp-Pfordt, *Cristallisation induite par cisaillement du MXD6 dans différentes formulations (additifs nucléants, fibres de verre)*, Ph.D. thesis, Université Claude Bernard, Lyon 1, 2006.
- [41] G. Lamberti, F. De Santis, V. Brucato, G. Titomanlio, Modeling the interactions between light and crystallizing polymer during fast cooling, *Appl. Phys. A* 78 (2004) 895–901, <https://doi.org/10.1007/s00339-003-2086-8>, 10.1007/s00339-003-2086-8.
- [42] G. Oukaci-Boukellal, *Détermination des paramètres non linéaires constitutifs de lois de comportement viscoélastique par mesures de champ dans des écoulements complexes*, Ph.D. thesis, Ecole des Mines de Paris, 2010.
- [43] F. De Santis, S. Adamovsky, G. Titomanlio, C. Schick, Scanning nanocalorimetry at high cooling rate of isotactic polypropylene, *Macromolecules* 39 (2006) 2562–2567, <https://doi.org/10.1021/ma052525n>.
- [44] D. Mileva, R. Androsch, E. Zhuravlev, C. Schick, B. Wunderlich, Homogeneous nucleation and mesophase formation in glassy isotactic polypropylene, *Polymer* 53 (2012) 277–282, <https://doi.org/10.1016/j.polymer.2011.11.064>, 10.1016/j.polymer.2011.11.064.
- [45] J.E. Schawe, Analysis of non-isothermal crystallization during cooling and reorganization during heating of isotactic polypropylene by fast scanning DSC, *Thermochim. Acta* 603 (2015) 85–93, <https://doi.org/10.1016/j.tca.2014.11.006>.
- [46] J.E. Schawe, P. Pötschke, I. Alig, Nucleation efficiency of fillers in polymer crystallization studied by fast scanning calorimetry: carbon nanotubes in polypropylene, *Polymer* 116 (2017) 160–172, <https://doi.org/10.1016/j.polymer.2017.03.072>.
- [47] S. Naudy, L. David, C. Rochas, R. Fulchiron, Shear induced crystallization of poly (m-xylylene adipamide) with and without nucleating additives, *Polymer* 48 (2007) 3273–3285, <https://doi.org/10.1016/j.polymer.2007.03.076>.
- [48] F.J. Stadler, J. Kaschta, H. Münstedt, F. Becker, M. Buback, Influence of molar mass distribution and long-chain branching on strain hardening of low density polyethylene, *Rheol. Acta* 48 (2009) 479–490, <https://doi.org/10.1007/s00397-008-0334-8>.
- [49] J. Amirdine, T. Burghelca, N. Boyard, J. Amirdine, T. Burghelca, N. Boyard, Effet d'une déformation extensionnelle sur la cinétique de cristallisation de polymères semi-cristallins to cite this version : HAL Id : hal-02420808, in: 21ème Journées Natl. sur les Compos. École Natl. Supérieure d'Arts Métiers - Bordeaux, 2019, 2019, Bordeaux, Talence, Fr, <https://hal.archives-ouvertes.fr/hal-02420808>.
- [50] Q. Liu, X. Sun, H. Li, S. Yan, Orientation-induced crystallization of isotactic polypropylene, *Polymer* 54 (2013) 4404–4421, <https://doi.org/10.1016/j.polymer.2013.04.066>.
- [51] B. Fiorentino, R. Fulchiron, J. Duchet-Rumeau, V. Bounor-Legaré, J.C. Majesté, Controlled shear-induced molecular orientation and crystallization in polypropylene/talc microcomposites – effects of the talc nature, *Polymer* 54 (2013) 2764–2775, <https://doi.org/10.1016/j.polymer.2013.03.057>, <http://www.sciencedirect.com/science/article/pii/S0032386113002760>.